LAND-COVER CLASSIFICATION OF TEHRAN USING L- AND C-BAND SYNTHETIC APERTURE RADAR IMAGERY

Homa Zakeri[1], Wen Liu[2], Fumio Yamazaki[3]

[1]Graduate Student, Chiba University, Chiba, Japan.
Email: homa.zakeri@chiba-u.jp
[2]Assistant Professor, Chiba University, Chiba, Japan
Email: wen.liu@chiba-u.jp
[3]Professor, Chiba University, Chiba, Japan
Email: fumio.yamazaki@faculty.chiba-u.jp

KEY WORDS: Land-cover, SAR imagery, unsupervised classification, texture measures, Tehran

ABSTRACT: Monitoring land-cover of urban areas is a main issue in several fields such as urban planning and seismic risk assessment. Detecting built-up and bare land areas in arid or semi-arid regions is quiet difficult by using multi-spectral optical images because of similarity of the spectral characteristics of grounds and building materials. On the contrary, synthetic aperture radar (SAR) images have possibility to overcome this issue because the backscatter depends on the material and geometry of different surface objects. The use of L- and C-band SAR images may have possibility to provide more information of the same objects in urban areas. In this paper, dual polarized data from ALOS-2 PALSAR-2 (HH, HV) with 6.2-m resolution and Sentinel-1 C-SAR (VV, VH) with 13.9-m resolution were used for an unsupervised classification analysis of land-cover in Tehran city, Iran, which has been growing very fast recently. Although the result of classification from the SAR images was better than that from optical images, some noise still remained in the result. Hence texture information was added to improve the classification. The result, which showed less noise by combining the texture measures with the backscattering intensity, was then compared with the visual inspection result of a high-resolution optical image and a reasonable level of accuracy was confirmed.

1. INTRODUCTION

Land-cover classification is a vital part of remotely sensed image analysis because it provides essential information in different applications such as urban planning, seismic risk assessment, ecological and urgent environmental monitoring in regional and global scales (Molch, 2000; Rathje and Adams, 2008; Yamazaki et al., 2011; Liu et al., 2013; Yamazaki and Liu, 2014). Synthetic Aperture Radar (SAR) with the ability of capturing images not only at daytime, but also at nighttime and under cloud-cover can extract objects' characteristics based on backscattering echo from them. Nowadays this technology, with dual or full polarization (HH, HV, VV and VH), is used widely for monitoring urban area and land-cover mapping since different polarizations have different sensitivities and scattering coefficients for the same target (Lee, 1999; Hokeman and Vissers, 2003; Matsuoka and Yamazaki, 2004). In this regard, texture measures, which depend on spatial relation, scale and orientation of objects, are important attributes for SAR image classification because various features such as built-up urban, soil, rock, and vegetation can be characterized easily. This is the advantage of using SAR images in land-cover classification than using multi-spectral optical images.

Tehran, the capital city of Iran, has been undergoing rapid changes in land-cover and land-use, like other metropolitan areas in developing countries. The population of Teheran has increased from 6,758,845 in 1996 to 12,183,391 in 2011, almost double only in 15 years, and thus it is considered as one of the fastest growing cities in the world. Since land-cover classification can support ecological monitoring, habitat assessment, wild-life management, global change monitoring, environmental impact assessment, state and local planning, hazardous waste remedial action, and regulatory policy development (Henderson and Lewis, 1998), urban area monitoring of Tehran seems necessary. According to the similarity of spectral signatures of soil and roof materials in built-up areas of Tehran, the accuracy of land-cover classification using optical images is expected not so high. On the other hand, a SAR image analysis using backscattering intensity data has the potential of accurate feature extraction in urban areas.

Many texture measures have been developed and properly used in satellite image analyses, which proved that the use of textural images improves the accuracy of land-cover classification (Haralick et al., 1973; Augusteijn et al., 1995; Shaban et al., 2001; Lu et al., 2008). The previous researches on texture feature extraction showed that the gray-level co-occurrence matrix (GLCM) is one of the trustworthy methods for classification (Clausi and Yue, 2004; Kandaswamy, 2005). Thus in this study, texture measures are applied to dual-polarized data of ALOS-2 PALSAR-2 (HH, HV) and Sentinel-1 C-SAR (VV, VH). Then, unsupervised land-cover classification of Tehran is carried out using the backscattering intensity and some texture measures, selected by a principal components analysis. This study attempts to examine the performance of SAR intensity data for land-cover classification in arid and semi-arid regions.

2. THE STUDY AREA AND DATASET

The study area of this research is Tehran, which is the capital city and a part of Tehran metropolitan area, as shown in **Figure 1**. Tehran is situated in the north-central Iran at the foot of the Alborz Mountains, and places on the sloping ground from the mountains in the north to the flat Great Salt desert in the south. As shown in **Table 1**, the population of the city had slightly increased from 6,058,207 in 1986 to 6,758,845 in 1996, but it rose significantly to 12,183,391 by 2011. Therefore the city needed more facilities for the residents. Due to this matter, several land-covers and land-uses emerged or changed into different ones.

The data employed in this research depicted in **Figure 1** were taken by ALOS-2, Sentinel-1, WorldView-3, and Landsat-8 satellites, which are operated by JAXA (Japan Aerospace Exploration Agency), ESA (European Space Agency), Digital Globe, and NASA (National Aeronautics and Space Administration), respectively. ALOS-2 was launched on May 24, 2014, with an enhanced L-band SAR sensor, PALSAR-2, and Sentinel-1 was launched on April 3, 2014 with C-SAR sensor in C-band. The both SAR images covering Tehran were in the ascending path with right-look, and by dual polarization. The ALOS-2 image taken on October 14, 2015 has HH and HV polarizations in Strip Map mode, the incident angle of 40.56º at the center of the image, and the spatial-resolution of 6.2 m. Sentinel-1 image captured on October 26, 2015 has VV and VH polarizations in the Interferometric Wide Swath mode, the incident angle of 34.02° at the center of the image, and the spatial-resolution of 13.9 m. The WorldView-3 image taken on October 4, 2015 consists of a panchromatic band (0.5-m resolution) and 8 multi-spectral bands (2.2-m resolution). The Landsat-8 image acquired on May 7, 2015 has a panchromatic band with 15-m resolution and 11 multi-spectral bands with 30-m resolution.

The SAR images were provided as the range and single-look azimuth compressed data with the processing level 1.1 ALOS-2 and level 1.0 Sentinel-1, which are represented by the complex I and Q channels to preserve the amplitude and phase information. After several pre-processing steps using the *Sentinel Toolboxes* free software, these images were projected on the WGS84 reference ellipsoid with a pixel spacing of 6.6 m. The radiometric calibration of each intensity image was carried out to get the backscattering coefficient (sigma naught, σ^0) in the ground range with the decibel (dB) unit, represented by the following equation.

$$\sigma^0 = 10.0 \log_{10}\left(k_s . |DN|^2\right) + 10.0 \log_{10}(\sin \theta_{loc}) \quad (1)$$

Where DN is the digital number of backscattering intensity, k_s the calibration factor, and θ_{loc} the local incidence angle. After this conversion, an adaptive filter (Lee, 1980) was applied to the original SAR images to reduce the speckle noise. Besides, the WorldView-3 image was also used as the truth data to extract the footprints of buildings after radiometric calibration and pan-sharpening processes.

Table 1 The change of population in Tehran

Year	1986	1991	1996	2006	2011
population	6,058,207	6,497,238	6,758,845	7,711,230	12,183,391

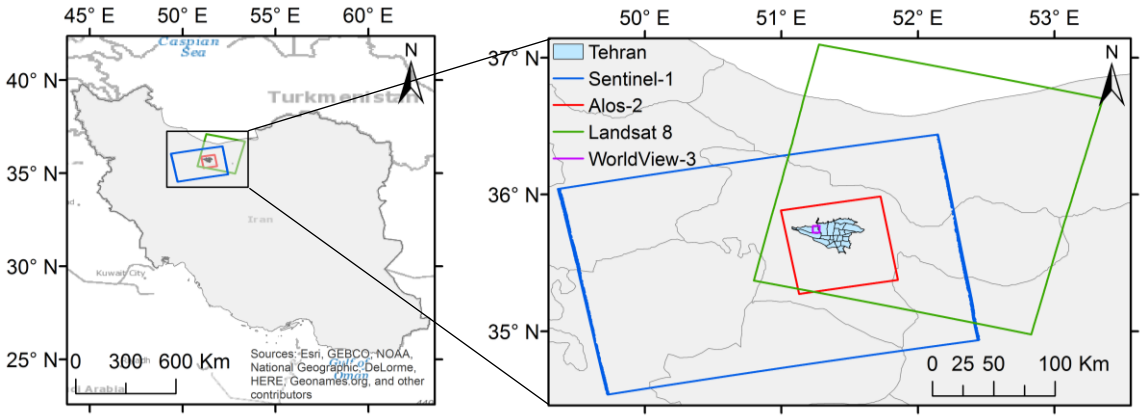

Figure 1 Location of Tehran and coverage of satellite images used in this study, including Sentinel-1 (blue frame) acquired on October 26, 2015; ALOS-2 (red frame) on October 14, 2015; Landsat-8 (green frame) on May 7, 2015; WorldView-3 (purple frame) on October 4, 2015.

3. METHODOLOGY

This study started with using the Landsat-8 multi-spectral optical image for land-cover classification of Tehran. The geographical situation of the study area makes it difficult to differentiate the urban area from the mountainous and desert area that surrounds Tehran, as shown in **Figure 2**. It reveals that the spectral reflectance characteristics of bare lands and built-up features are remarkably similar while other signatures such as roads, vegetation, and water show different characteristics. Thus, SAR images with the capability of obtaining ground surface information based on backscatter were chosen to conduct the study following the flowchart shown in **Figure 3**.

After applying the preprocessing steps, two dual polarizations, HH and HV for ALOS-2 and VV and VH for Sentinel-1, were stacked for computing texture measures. The previous researches have shown that the texture measures are vital information from radar imagery (Ulaby et al., 1982; Dell'Aqua and Gamba, 2003). Among several statistical texture methods proposed before, the gray-level co-occurrence matrix (GLCM) is one of the most powerful one for land-cover monitoring (Haralic et al., 1973). This measure represents the spatial distribution of the gray-level value and its frequency with another one in a specific displacement at (x, y) and angles (0º, 45º, 90º, and 135º). From a sub-image of a given window size, $I(x,y)$, the GLCM is a matrix P with size N_g x N_g (N_g: the number of gray-levels) whose $P(i, j)$ element ($1 \le i \le N_g$; $1 \le j \le N_g$) contains the number of times a point with gray-level g_i occurring in a set of relative positions (based on the displacement and the angle mentioned before) to another point with gray-level g_i. In this study, ten textural features in angle 0º, distance 1, and a window size of 7 x 7 were used for classification as follows:

$$\text{Angular Second Moment} = \sum_i \sum_j \{P(i, j)\}^2 \tag{2.1}$$

$$\text{Contrast} = \sum_{n=0}^{N_{g-1}} n^2 \left\{ \sum_{\substack{i=1 \\ |i-j|=n}}^{N_g} \sum_{j=1}^{N_g} P(i, j) \right\} \tag{2.2}$$

$$\text{Correlation} = \frac{\sum_i \sum_j (ij) P(i, j) - \mu_x - \mu_y}{\sigma_x \sigma_y} \tag{2.3}$$

$$\text{Homogeneity} = \sum_i \sum_j \frac{1}{1 + (i - j)^2} P(i, j) \tag{2.4}$$

$$\text{Variance} = \sum_i \sum_j (i - \mu)^2 P(i, j) \tag{2.5}$$

$$\text{Mean} = \sum_{i=2}^{2N_g} i p_{x+y}(i) \tag{2.6}$$

$$\text{Entropy} = -\sum_i P \log (P(i, j)) \tag{2.7}$$

$$\text{Energy} = \sum_i \sum_j P(i, j)^2 \tag{2.8}$$

$$\text{Maximum Probability} = \max(P_{ij}) \tag{2.9}$$

$$\text{Dissimilarity} = \sum_{i, j=0}^{N_g - 1} P_{i, j} (-\ln P_{i, j}) \tag{2.10}$$

Where $p(i, j)$ is the (i, j)-th entry in a normalized gray-tone spatial dependence matrix ($P(i, j)/R$); R is usually the total sum of P; $p_x(i) = \sum_{j=1}^{Ng} P(i, j)$ is the i-th entry in the marginal-probability matrix obtained by summing the rows of $p(i, j)$; μ_x, μ_y, σ_x and σ_y are the means and standard deviations of p_x and p_y.

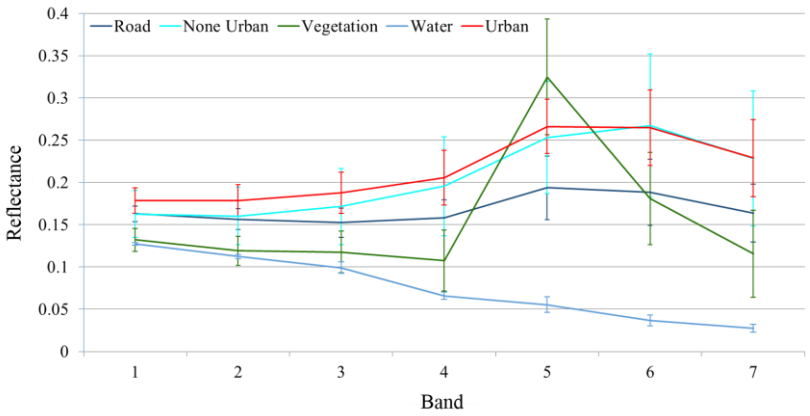

Figure 2 Spectral signature of different land-cover types for the Landsat-8 image of Tehran

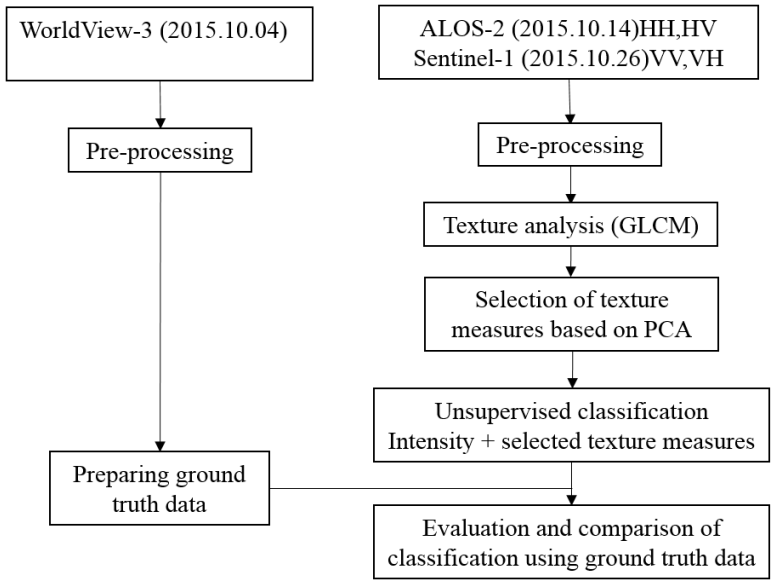

Figure 3 Flowchart of land-cover classification using SAR data in this study

Three texture features: *Contrast*, *Variance* and *Mean* of the sigma naught images, were selected based on the highest participation factor of them from the first three components in the principal component analysis. The contrast depicts the amount of local variation pixel values, the variance illustrates the distance of each pixel from the average and the mean is the average of the whole pixel values. Then, unsupervised classification using the K-mean clustering algorithm was applied to two cases: the first case where only intensity image of ALOS-2 and Sentinel-1 (HH, HV, VV, and VH) were used, and the second case where the three texture measures of the sigma naught were also employed in unsupervised classification. The K-mean clustering is one of the most well-known algorithms which identifies k cluster from the distance measure of values. Different numbers of classes were tested (five to ten) in computing the K-mean algorithm. Seven classes were chosen in this method because the number of classes less than seven did not cluster features well and more than seven classes included a lot of salt-and-pepper noises.

To check the accuracy of unsupervised classification using the K-mean algorithm, truth data were obtained from the WorldView-3 image for three different regions of land-covers (built-up, bare land, and vegetation) in the study area. Then the pixel values of each land-cover class were extracted and were compared with the ones in the truth data.

4. THE RESULT AND DISCUSSION

In order to evaluate the capability of texture measures, samples of the sigma naught value and their texture measures were obtained from several regions of interest with the three different land-covers (build-up, bare land, vegetation). **Figure 4** shows the scatter plots of the sigma naught and their textures from the dual polarizations of ALOS-2 (HH and HV) and **Figure 5** for those for Setinel-1(VV and VH). In these figures, built-up, bare land, vegetation areas are shown in black, yellow and green dots, respectively. Besides, the average of each group is depicted as red, cyan and pink plus mark. As can be observed in **Figure 4a** and **Figure 5a**, there are overlaps among the sigma naught values.

But, the texture values (**Figure 4b-4d** and **Figure 5b-5d**) show moderate levels of separation among built-up, bare land and vegetation pixels. Moreover the average for each group of texture measure is seperated better than that of the sigma naught itself.

Therefore, the texture measures seem to be effective in differentiating built-up and bare land areas. In case of texture measures for bare land and vegetation from HH and HV polarizations (**Figure 4b-4d**), only slight improvements are seen, compared with the scatter plot of sigma naught valus (**Figure 4a**). However, the same two features overlap in the Sentinel-1's VV and VH images not only for the sigma naught (**Figure 5a**), but also for the texture measures, as shown in **Figure 5b-5d**.

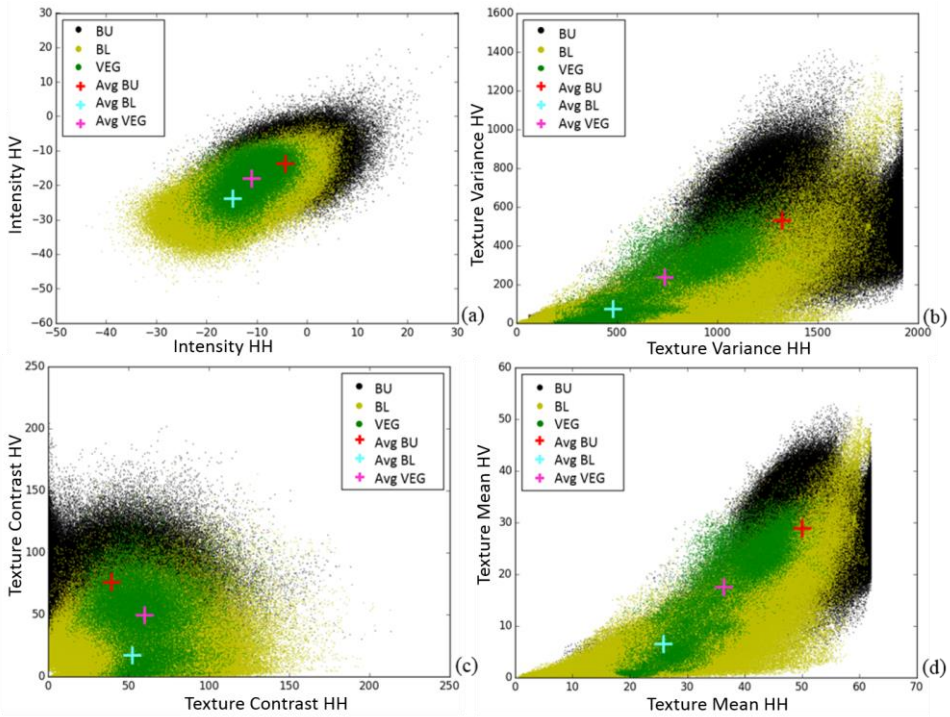

Figure 4 Scatter plots of ALOS-2's sigma naught values (HH, HV) and their texture measures

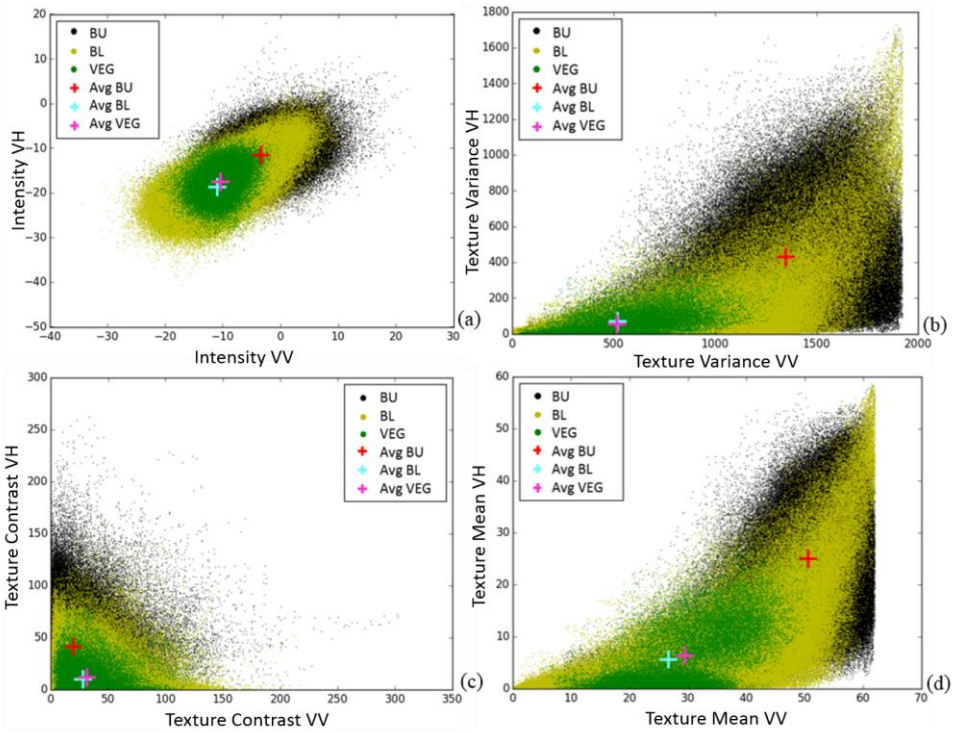

Figure 5 Scatter plots of Sentinel-1's sigma naught values (VV, VH) and their texture measures

Considering the improvement in differentiating built-up and bare land areas when the GLCM texture measures were used, which is the main objective of this study, unsupervised classification using the K-mean algorithm with 7 classes was carried out. **Figure 6** shows the unsupervised classification results of Tehran and its surrounding areas. **Figure 6a**, **6c**, and **6e** depict the results of classification using L-, C-, and L+C-band intensities, respectively. **Figure 6b**, **6d**, and **6f** illustrate the classification when the texture measures were included together with the L-, C-, and L+C-band intensities. The results with the texture measures show less noise compared with those without them.

In order to evaluate the results of unsupervised classification, three districts representing different building densities: low-, medium, and high-density, were selected as shown in **Figure 7.** These districts are located in the north-west of Tehran, a part of a newest region as a result of city expansion. The truth data were obtained based on visual inspection from the WorldView-3 image. In this paper we evaluate only the results of **Figure 6e** and **6f**.

Figure 8 shows the optical image (left), the results of unsupervised classification without using textures (center) and with using them (right), for three building densities. As mentioned before, the results of unsupervised classification without texture shown in **Figure 8b**, **8e**, and **8h** illustrate high level of noise that makes difficult to distinguish the border lines between different classes. On the contrary, **Figure 8c**, **8f**, and **8i** show the border lines of land-covers, and the pixel values of different classes look more uniform with less noise and are comparable with the truth data.

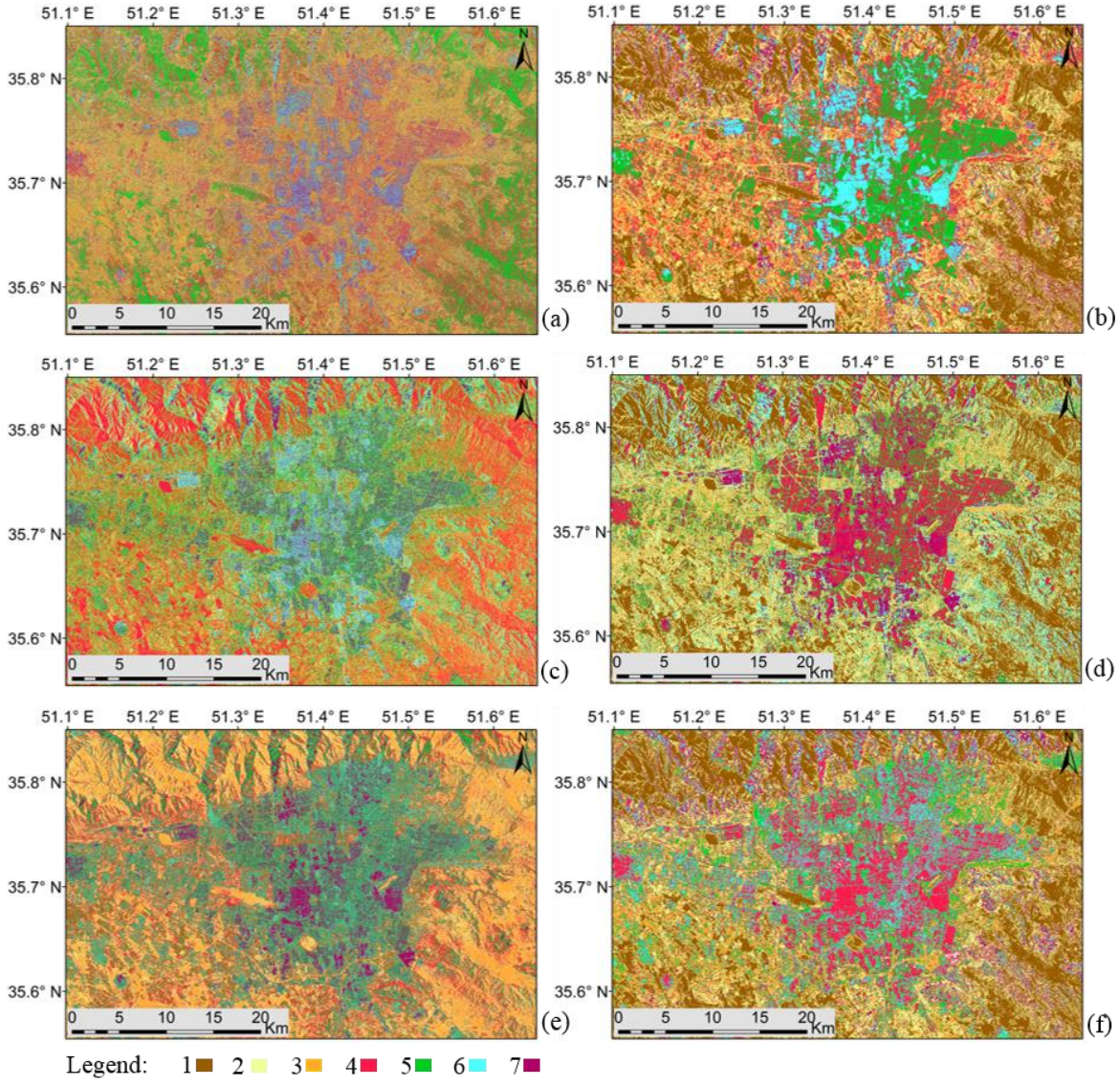

Figure 6 The results of unsupervised classification of Tehran using the K-mean method with 7 classes; (a), (c), and (e) show the cases using the sigma naught values from ALOS-2 (HH, HV), Sentinel-1(VV, VH), and the both of them (HH, HV, VV, and VH); (b), (d), and (f) are the cases using the combination of the sigma naught values and their texture measures (Variance, Contrast, and Mean), for ALOS -2 (HH, HV), Sentinel-1(VV,VH), and the both (HH, HV, VV, and VH).

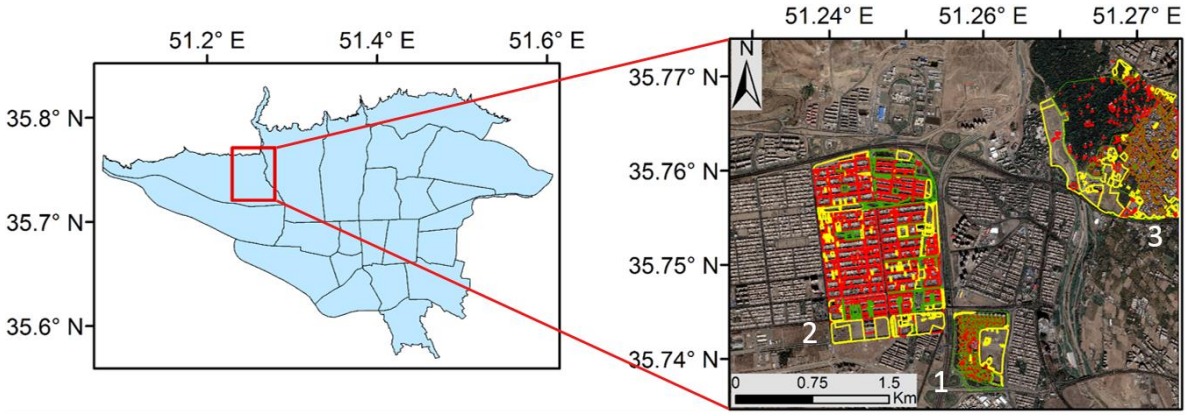

Figure 7 Close-up of the study area in Tehran. Three types of districts, 1) low-, 2) medium-, and 3) high-density residential.

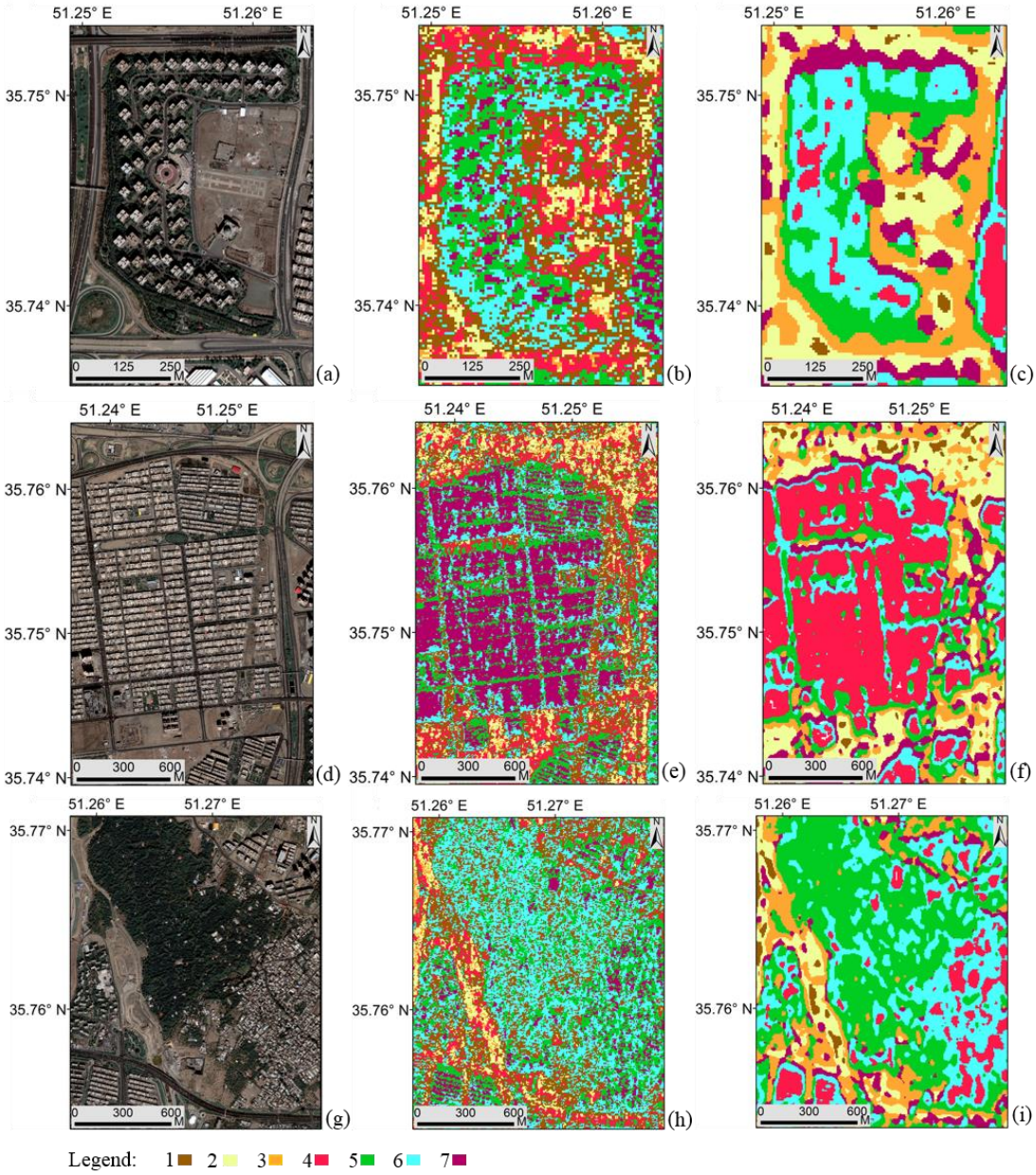

Figure 8 Unsupervised classification for low-, medium-, and high-density residential districts in Tehran. (a), (d), and (g) show the optical image, (b), (e), and (h) are the results using only the sigma naught values (HH, HV, VV, and VH) of ALOS -2 and Sentinel-1; (c), (f), and (i) are the results using both the sigma naught values and their texture measures (Variance, Contrast, Mean).

Table 2 The result for the low density district

Class	Intensity			Total
	Built-up	Bare Land	Vegetation	
	Pixel	Pixel	Pixel	
Built-up	1178	79	1051	2308
Bare Land	348	1137	377	1862
Vegetation	1398	844	1966	4208
Total	2924	2060	3394	8378
Overall classification accuracy (%):			51.1	

Class	Intensity + Texture			Total
	Built-up	Bare Land	Vegetation	
	Pixel	Pixel	Pixel	
Built-up	1566	27	1245	2838
Bare Land	204	1287	383	1874
Vegetation	1154	746	1766	3666
Total	2924	2060	3394	8378
Overall classification accuracy (%):			55.1	

Table 3 The result for the medium density district

Class	Intensity			Total
	Built-up	Bare Land	Vegetation	
	Pixel	Pixel	Pixel	
Built-up	25110	2390	1892	29392
Bare Land	1617	2065	1562	5244
Vegetation	7174	1938	3022	12134
Total	33901	6393	6476	46770
Overall classification accuracy (%):			64.6	

Class	Intensity + Texture			Total
	Built-up	Bare Land	Vegetation	
	Pixel	Pixel	Pixel	
Built-up	26849	2114	1694	30657
Bare Land	1483	2778	2216	6477
Vegetation	5534	1513	2589	9636
Total	33866	6405	6499	46770
Overall classification accuracy (%):			68.9	

Table 4 The result for the high density district

Class	Intensity			Total
	Built-up	Bare Land	Vegetation	
	Pixel	Pixel	Pixel	
Built-up	6872	675	3666	11213
Bare Land	294	2221	819	3334
Vegetation	6377	1906	12834	21117
Total	13543	4802	17319	35664
Overall classification accuracy (%):			61.5	

Class	Intensity + Texture			Total
	Built-up	Bare Land	Vegetation	
	Pixel	Pixel	Pixel	
Built-up	10236	685	4400	15321
Bare Land	183	2594	601	3378
Vegetation	3124	1523	12318	16965
Total	13543	4802	17319	35664
Overall classification accuracy (%):			70.5	

To evaluate the accuracy of the classification method, the unsupervised classification results (the number of pixels for seven classes) were compared with the truth data for the cases without and with using the texture measures. Before evaluating the results, the class numbers from unsupervised classification were merged into three groups: build-up, bare land, and vegetation. The largest pixel number for each unsupervised class was selected to connect with the land-cover that it belongs, for the three districts.

Thus, for the case of classification without texture measures, classes 5 and 7 were assigned as built-up, classes 2, 3 and 4 as bare land, and class 1 and 6 as vegetation. Besides, in case of unsupervised classification with texture measures, it is easier to select the highest pixel numbers in each class for the three density districts than classification without texture measures. Accordingly, classes 1, 2 and 7 were selected as bare land, classes 3 and 5 were chosen as vegetation, and classes 4 and 6 include large parts of built-up. When the texture measures are included, the number of cases in which overlapping of classes occur was reduced.

Confusion matrix is calculated and presented in
Table 2-4 for the three density districts. Diagonal elements refer to the number of pixels that were classified correctly as built-up, bare land and vegetation out of 8,378, 46,770 and 35,664 truth pixels in low-, medium- and high-dense districts. Overall classification accuracy, the sum of the diagonal elements of the confusion matrix divided by the total amount of pixels, was obtained in order to compare the results without and with texture. The overall classification accuracy increased in percentage from 51 to 55 for the low-density, from 65 to 69 for the medium-density, and from 62 to 71 for the high-density districts. It is worth to mention that due to the effects of shadow and layover in SAR images, the results of classification were shifted to the ground-range direction in different magnitudes. But, using the WorldView-3 image, we could only apply an average shift to each dense area. Therefore, the result in the tables should be considered as a reference.

5. CONCLUSION

In this study, the GLCM texture measures were applied to evaluate its potential use for improving unsupervised classification of SAR intensity images for urban areas. In this purpose, Tehran was selected as the study area because of its fast expansion. Due to the spectral signatures' similarity of soil and roof material in built-up regions from a multi-spectral optical image analysis, SAR images with capability of obtaining features characteristics based on radar backscatter were chosen. Dual polarized data from L-band ALOS-2 (HH, HV) and C-band Sentinel-1 (VV, VH) were employed and the texture properties were calculated. Three texture measures were selected based on the result of a principal component analysis. Then, the K- mean clustering algorithm was introduced for two cases: without and with texture measures. The result of unsupervised classification with texture measures was found to be superior to the one without texture in two main aspects: less level of noise and clearer borders of land-covers.

The results of unsupervised classification were compared with the truth data obtained from visual inspection of a WorlView-3 image for three different urban density districts: low-, medium-, and high-density. The results showed that the texture measures improve the capability of unsupervised classification. However, the classification was not optimal mainly because unsupervised classification is a basic method that is performed in an early stage of land-cover classification. Supervised classification using training data would be more conclusive; however this issue will be considered in a future study.

ACKNOWLEDGMENT

The ALOS PALSAR-2 data used in this study are owned by Japan Aerospace Exploration Agency (JAXA), and were provided through the JAXA's ALOS-2 research program (RA4, PI No. 1503). The Pleiades images are owned by Airbus Defence and Space and licensed to Chiba University.

REFERENCES

Augusteijn, M. F., Clemens, L. E., Shaw, K. A., 1995. Performance Evaluation of Texture Measures for Ground Cover Identification in Satellite Images by Means of a Neural Network Classifier, IEEE Transactions on Geoscience and Remote Sensing, 33(3), pp. 616-625.

Clausi, D. A., Yue, B., 2004. Comparing Co-Occurrence Probabilities and Markov Random Fields for Texture Analysis of SAR Sea Ice Imagery, IEEE Transactions on Geoscience and Remote Sensing, 42(1), pp. 215-228.

Dell'Aqua, F. and Gamba, P., 2003. Texture-Based Characterization of Urban Environments on Satellite SAR Images, IEEE Transactions on Geoscience and Remote Sensing, 28, pp. 540-552.

Henderson, F.M., 1998. Manual of remote sensing: Principle and applications of imaging radar, edited by Reyrson, R.A., New York.

Haralick, R.M., Shanmugam, K., and Dinstein, I., 1973.Textural feature for image classification, IEEE Transactions on Systems, Man and Cybernetics, SMC-3, No.6, pp. 610-621.

Hoekman, D.H., Vissers, M.A.M., 2003. A New Polarimetric Classification Approach Evaluated for Agricultural Crops, IEEE Transactions on Geoscience and Remote Sensing, 41(12), pp. 2881-2889.

Kandaswamy, U., Adjeroh, D. A., Lee, M. C., 2005. Efficient Texture Analysis of SAR Imagery, IEEE Transactions on Geoscience and Remote Sensing, 43(9), pp. 2075-2083.

Lee, J.S., 1980. Digital Image Enhancement and Noise Filtering by Use of Local Statistics, IEEE Transaction on Pattern Analysis and Machine Intelligence, 2(2), pp. 165-168.

Lee, J.S., Grunes, M.R., De Grandi, G., 1999. Polarimetric SAR Speckle Filtering and Its Implication for Classification, IEEE Transactions on Geoscience and Remote Sensing, 37(5), pp. 2363-2373.

Liu, W., Yamazaki, F., Goken, H., Koshimura, S., 2013. Extraction of Tsunami-Flooded Areas and Damaged Buildings in the 2011 Tohoku-Oki Earthquake from TerraSAR-X Intensity Images, Earthquake Spectra, EERI, 29 (S1), pp. S183-S200.

Lu, D., Batistella, M., Moran, E., De Miranda, E. E., 2008. A Comparative Study of Landsat TM and SPOT HRG Images for Vegetation Classification in the Brazilian Amazon, Photogrammetric Engineering & Remote Sensing, 70, pp. 311-321.

Matsuoka, M., and Yamazaki, F., 2004. Use of satellite SAR Intensity Imagery for Detection Building Areas Damage due to Earthquake, Earthquake Spectra, 20, pp. 975-994.

Molch, K., 2009. Radar Earth Observation Imagery for Urban Area Characterisation, JRC scientific and technical reports.

Rathje, E., Adams, B.J., 2008. The Role of Remote Sensing in Earthquake Science and Engineering: Opportunities and Challenges, Earthquake Spectra, 24(2), pp. 471–492.

Shaban, M. A., and Dikshit, O., 2001. Improvement of Classification in Urban Areas by the Use of Textural Features: The Case Study of Lucknow City, Uttar Pradesh, International Journal of Remote Sensing, 22(4), pp. 565–593.

Ulaby, F.T., Moore, R.K. and Fung, A.K., 1982. Microwave Remote Sensing Active and Passive from Theory to Applications, III, Artech House, Massachusetts, pp. 1115-1120.

Yamazaki, F., Inoue, H., Liu, W., 2011. Characteristics of SAR Backscattering Intensity and its Application To Earthquake Damage Detection, Computational Stochastic Mechanics, Edited by G. Deodatis, P. D. Spanos, Research Publishing, pp. 602-606.

Yamazaki, F., and Liu, W., 2014. Urban Change Monitoring: Multi-temporal SAR Images, Encyclopedia of Earthquake Engineering, Springer-Verlag Berlin Heidelberg, pp. 1-13.